Original Research

Continuous Arterial Spin Labeling Using a Train of Adiabatic Inversion Pulses

Bradford A. Moffat, PhD, Thomas L. Chenevert, PhD,* Daniel E. Hall, MSc, Alnawaz Rehemtulla, PhD, and Brian D. Ross, PhD

Purpose: To develop a simple and robust magnetic resonance imaging (MRI) pulse sequence for the quantitative measurement of blood flow in the brain and cerebral tumors that has practical implementation advantages over currently used continuous arterial spin labeling (CASL) schemes.

Materials and Methods: Presented here is a single-coil protocol that uses a train of hyperbolic secant inversion pulses to produce continuous arterial spin inversion for perfusion weighting of fast spin echo images. Flow maps of normal rat brains and those containing a 9L gliosarcoma orthotopic tumor model conditions were acquired with and without carbogen.

Results: The perfusion-weighted images have reduced magnetization transfer signal degradation as compared to the traditional single-coil CASL while avoiding the use of a more complex two-coil CASL technique. Blood flow measurements in tumor and normal brain tissue were consistent with those previously reported by other CASL techniques. Contralateral and normal brain showed increased blood flow with carbogen breathing, while tumor tissue lacked the same CO_2 reactivity.

Conclusion: This variation of the CASL technique is a quantitative, robust, and practical single-coil method for measuring blood flow. This CASL method does not require specialized radiofrequency coils or amplifiers that are not routinely used for anatomic imaging of the brain, therefore allowing these flow measurements to be easily incorporated into traditional rodent neuroimaging protocols.

Key Words: MRI; arterial spin tagging; arterial spin labeling; brain tumor; carbogen; blood flow
J. Magn. Reson. Imaging 2005;21:290–296.

BLOOD FLOW is an important physiologic function that affects tumor viability, metastatic potential, delivery access of chemotherapeutic agents, and tissue oxygenation, which impacts radiosensitivity. Conversely, anticancer therapies can modulate blood flow by design, or indirectly by damage to the vasculature. Therefore, characterization of blood flow is important for our understanding of tumor physiology and mechanisms of therapeutic activity, as well as assisting in design and monitoring of new therapeutic trials. Moreover, practical methods for noninvasively imaging tumor blood flow would be valuable in preclinical studies and could potentially expedite translation of successful strategies into clinical application.

Over the last eight to 10 years, several elegant magnetic resonance imaging (MRI) methods have been developed to measure tissue blood flow (TBF) in quantitative and semiquantitative terms (1–6). MR perfusion imaging based on the transient passage of a T2* contrast agent is popular in human exams due to its speed, robustness, and simplicity. This approach generates maps of cerebral blood volume (CBV) and mean transit time (MTT), which are parameters related to tissue perfusion. Deconvolution of the arterial input function, along with corrections for agent recirculation and/or leakage, are steps toward absolute quantification of cerebral blood flow (CBF), although in clinical practice often only the "relative" CBV, MTT, and CBF are available. In rodent imaging, however, perfusion imaging by this approach is technically more challenging for several reasons. First, it is difficult to sample the transient contrast agent bolus at sufficient temporal resolution due to short cerebral circulation time (~1–2 seconds) in rodents compared to human (~10 seconds), even when echo planar imaging is utilized. This method also requires a venous injection of contrast material. While tail vein catheterization is certainly feasible and reliable in skilled hands, it is not trivial for some animal models. It is particularly problematic when repeated tail injections are required on each animal in serial studies, such as in our application.

For the reasons stated above, arterial spin labeling (ASL) schemes are an attractive alternative for serial study of rodent brain tumor models. The essential element of ASL is to "tag" the longitudinal magnetization of the blood prior to its entry into the imaged slice. As detailed in several reports, the spin perfusion component can be derived by appropriate mathematical combination of tagged and control (untagged) data. In a

Department of Radiology, University of Michigan, Ann Arbor, Michigan.
Contract grant sponsor: NIH; Contract grant numbers: PO1-CA85878-01, R24-CA83099, P50CA93990.
A portion of this work was presented at the 10th Annual Meeting of ISMRM, Honolulu, 2002.
*Address reprint requests to: T.L.C., 1500 E. Medical Center Drive, Department of Radiology - MRI, University of Michigan Health System, Ann Arbor MI 48109-0030. E-mail: tlchenev@umich.edu
Received January 8, 2004; Accepted November 17, 2004.
DOI 10.1002/jmri.20268
Published online in Wiley InterScience (www.interscience.wiley.com).

recent review of brain perfusion imaging (1) arterial spin labeled MRI were classified by two general approaches: pulsed ASL and continuous ASL.

While pulsed ASL techniques (1) do not require any specialized hardware that is not otherwise available on standard MR scanners, they generally have lower signal-to-noise ratio (SNR) than continuous ASL sequences (2). Pulsed techniques also require careful consideration of slice profiles used for spin tagging relative to image section definition to avoid artifact within blood flow maps. For example, the flow-sensitive alternating inversion recovery (FAIR) approach (6) is a well-known pulsed ASL method that combines slice-selective and non-slice-selective inversion datasets. In relation to rodent imaging, the relatively short transit time of the blood from the heart to the brain requires that the non-slice-selective inversion completely encompass the body or at least the torso. Therefore, a whole-body volume coil is preferred to transmit tag pulses. Unfortunately, MR perfusion images are typically limited by a low SNR; thus, signal reception with a small volume or surface coil is recommended. Certainly these requirements are satisfied by two-coil systems comprised of a large-volume transmit and a small surface reception coils, but physical setup and decoupling of these coils further adds to the complexity of this approach.

The aim of this work was to develop a new protocol for measuring perfusion in the rat brain that is simple, robust, and compatible with requirements posed by other imaging elements of neuroimaging protocols. In this method, perfusion weighting is achieved by pseudocontinuous ASL. The 9L rat brain tumor has been widely used as a preclinical model for the evaluation of experimental antitumor therapies. The 9L model presents a challenge for perfusion imaging, however, since despite being considered a "vascular" tumor, it is characterized by low blood flow of 20–60 mL/100 g/minute (3) relative to normal brain of approximately 100–200 mL/100 g/minute (3,4,7,8). The sensitivity of this technique for measuring changes in perfusion was assessed by alternating the air/carbogen inhalation mixture, which is known to modulate CBF.

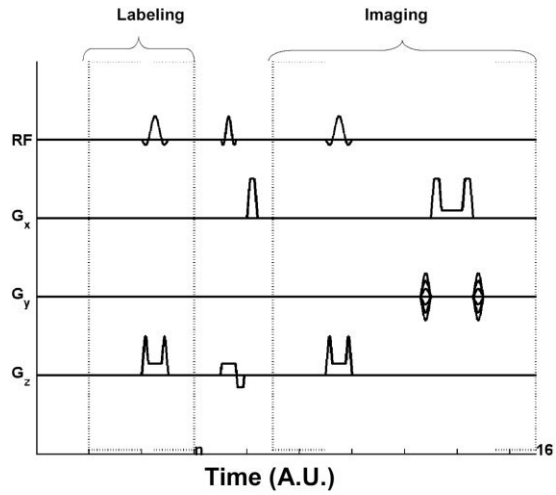

Figure 1. Timing diagram (in arbitrary units [AU] not drawn to scale) of the perfusion-weighted CASL FSE pulse sequence. Arterial spin tagging is achieved by an initial train of HS inversion RF pulses. The number of HS pulses (n) is usually between 50 and 65 equally spaced over three seconds. The arterial spin tagging is then followed by a standard FSE imaging sequence.

MATERIALS AND METHODS

MRI Acquisition

The proposed MR perfusion imaging method was implemented by preweighting a fast spin echo (FSE) sequence (Fig. 1) with a train of slice-selective hyperbolic secant (HS) inversion pulses located inferiorly from the image plane. The location of the HS excitation band was set within the radiofrequency (RF) sensitivity of the quadrature birdcage coil (4 cm diameter by 5 cm length) normally used for rat brain imaging on our 7-T MRI system. The RF power of the HS pulses was set to achieve inversion at the desired location by inspection of the phase-sensitive one-dimensional object profile along the body-axis. The HS pulses had an 8 kHz bandwidth, an adiabatic selectivity of 1/15.79, and maximum amplitude of 903.5 milliGauss (mG) (10^{-7} Tesla). Inversion pulse frequency offset and gradient strength were set to provide 8-mm-wide tag/control bands centered $\pm$15 mm from the center of the imaged slice. To approximate continuous ASL labeling conditions, a long train of HS tag pulses was applied over a sufficient period to allow labeled blood to exchange with tissue water in the imaged slice. In the rat, blood transit and exchange time was expected to be within a few seconds. The labeling period can be extended further but possible gains are diminished since the label undergoes T1 decay. In these experiments, the labeling period was held fixed at three seconds, which is the same as previously used in other CASL experiments (3). The HS pulses were uniformly distributed over this three-second interval with the quantity of HS pulses used as the single independent variable for optimization. Simplistically, the pulse-to-pulse period should match the time to replenish each plug parcel of blood passing through the inversion zone. In reality, arterial blood flow is pulsatile and not plug-like. Nevertheless, the number of HS pulses can be optimized for a given animal by maximizing the signal difference between tag and control conditions in the imaged slice. This step was performed by alternating between tag and control conditions and inspecting the one-dimensional projection of the imaged slice as a function of HS pulse quantity. The one-dimensional signal profiles integrated over a range known to contain the brain provided an efficient means to optimize the number of ASL inversion pulses for each animal by plotting the relative difference between the control and arterial spin labeled profiles plotted as a function of quantity labeling pulses (Fig. 2). It was determined that 50 to 70 (depending on the individual rat) 2-msec HS pulses were needed to obtain maximum labeling efficiency. It is apparent from Fig. 2 that the labeling efficiency plateaus; therefore, the minimum number of HS pulses to reach this plateau was used to reduce specific absorption rate (SAR) and magnetization transfer (MT) effects. The MT degradation of the

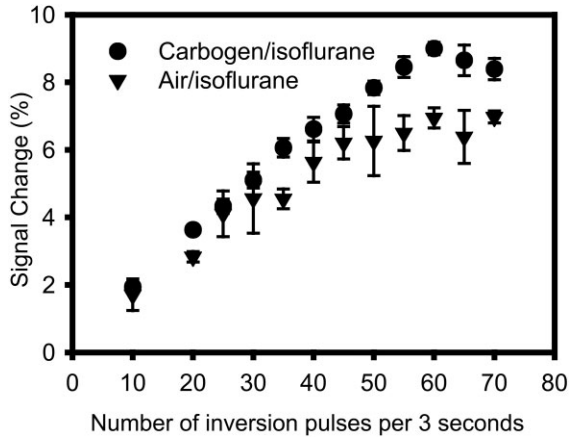

Figure 2. A plot showing the relative difference of the rat brain NMR signal between control and arterial spin tagging for the CASL pulse sequence as a function of the number of HS pulses during a three-second labeling period.

image signal intensity was quantified by calculating the percent signal difference between each control projection and a projection with zero HS inversion pulses.

While the above one-dimensional method allows for efficient optimization of the inversion efficiency (α), it does not readily provide its quantification. Therefore, inversion efficiency was measured in the necks of four animals. These animals were positioned with the carotid arteries nearer the center of the RF coil than normally positioned for brain imaging. The inversion efficiency was calculated using a gradient-echo method similar to that previously reported (9). Briefly, one slice-selective HS inversion pulse positioned inferior (or symmetrically superior) to the imaged slice was applied per TR of a flow-compensated two-dimensional gradient-echo sequence. To emulate tag conditions in the CASL imaging sequence, the gradient-echo TR time was varied from 15 to 75 msec, equivalent to 200 to 40 HS pulses per three-second period, respectively. For comparative purposes, data were also acquired using a sinc-shaped inversion pulse to assess the benefit of adiabatic pulses on inversion efficiency. The inversion efficiency was calculated using the following equation:

$$\alpha = \frac{(S_0^c - S_1^c)}{2S_0^c}, \qquad (1)$$

where S_0^c is the signal intensity from the carotid arteries when the inversion pulses invert spins 8 mm downstream from the image plane and S_1^c is the signal intensity of the carotid arteries when the inversion pulses invert spins 8 mm upstream from the image plane. The slice thickness of the inversion band was 8 mm and the image slice thickness was 1 mm. Echo time was held constant at 5 msec, the image field of view (FOV) was 3 × 3 cm, and the image matrix size was 256 × 256. Pixel-wise maps of the inversion efficiency were generated (Fig. 3) as color overlays on the gradient echo images, and mean inversion efficiency for each TR period and each animal was calculated from regions of interest (ROIs) defined on the carotid arteries.

To acquire flow maps, CASL was accomplished with FSE based imaging sequence. Each three-second labeling period ended immediately before the initial 90° pulse of a 16-echo, 128-phase FSE sequence, with a TR/TE_{eff} of 4000/14 msec, 2 mm slice thickness, and eight transients. The images were acquired with a 3 × 3 cm FOV, and the 128 × 128 acquisition matrix was subsequently zero-filled to 256 × 256. A T_1 map of the imaged slice was also acquired with a magnetization inversion-prepared 16-echo, 64-phase encoding FSE sequence. The image acquisition matrices (128 × 64) were zero-filled to 256 × 256 so that the resulting pixel size was identical to that of the perfusion weighted images. Five different inversion times, T_i, were used with two transients and TR/TE_{eff} of 10,000/14 msec. All imaging was performed on a horizontal bore 7-T Varian Unity Inova imaging system. Perfusion images or TBF maps were calculated using the formula for continuous labeling (5):

$$TBF = \frac{\lambda}{T_1}\frac{(S_0 - S_1)}{2\alpha S_0} \qquad (2)$$

where λ is the blood/tissue partition function (assumed to be 0.9), T_1 is the tissue longitudinal relaxation time, S_0 and S_1 are the image signals with inversion pulses applied to control and tag zones, respectively, and α is the efficiency of the inversion pulses.

Animal Model

Rat 9L gliosarcoma cells were grown as monolayers in minimal essential medium supplemented with 10% fetal calf serum, 100 IU/mL penicillin, and 100 μg/mL streptomycin at 37°C in a 95/5% air/CO_2 atmosphere.

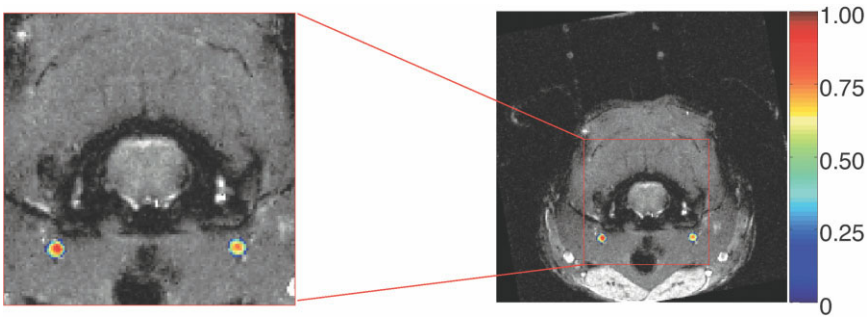

Figure 3. Inversion efficiency quantitative color map overlaid on a transverse gradient echo image through the neck of a rat. The distribution of inversion efficiency within the carotids can be observed in the expanded region (left). TR/TE = 55/5 msec, slice thickness = 1 mm.

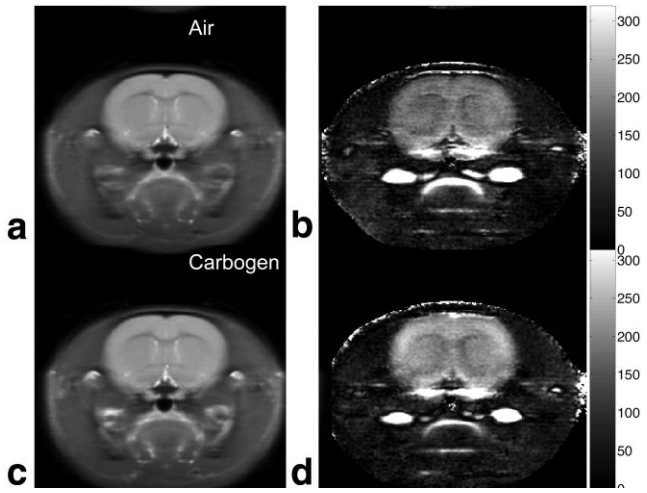

Figure 4. An example of the CASL imaging results for a normal rat brain while the animal was breathing air and isoflurane (**a** and **b**), and while it was breathing carbogen and isoflurane (**c** and **d**). The FSE proton density weighted images with arterial spin tagging by CASL (a and c) are shown on the left, while the corresponding TBF (mL/100 g/minute) images (b and d), are shown on the right.

Intracerebral 9L tumors were induced in male Fischer 344 rats weighing between 125 and 150 g as previously described (10). Briefly, 10^5 9L cells were implanted in the right forebrain at a depth of 3 mm through a 1 mm burr hole under anesthesia. Tumors were allowed to grow to reach approximately 100 μL (approximately 14–20 days post implantation). For MRI examination, rats were anesthetized with 1.5% isoflurane gas delivered by air or carbogen (95% oxygen + 5% carbon dioxide) at a rate of 4 liters/minute flowing over the nose/head. Animal body temperature was maintained at 37°C using a water pad and re-circulating heated water bath.

The CASL protocol was used to produce quantitative flow maps of the rat brain in healthy Fisher 344 rat brains ($N = 4$) and 9L tumor-bearing rats ($N = 5$).

RESULTS

Animal-specific tuning of the CASL method involves determining the appropriate rate to apply HS tag pulses during the labeling period. As described, an alternating series of tag/control one-dimensional profiles of the brain are acquired as a function of quantity of HS pulses applied during the three-second labeling period. Figure 2 illustrates relative signal change vs. pulse count for a rat breathing both air/isoflurane and carbogen/isoflurane. From this plot, it can be seen that signal change (or labeling efficiency) increases with increasing number of hyperbolic secant inversion (HSI) pulses to a plateau. For all animals, the number of pulses at which this plateau starts is between 50 and 60 per three-second tag period. From integrated regions over these profiles the percentage decrease in signal due to MT effects was estimated. As expected, the MT effect increased with increasing number of inversion pulses. The maximum MT degradation observed with the 70 pulses was 35 ± 5%. Therefore to reduce MT degradation and energy deposition the minimum number of pulses to reach the plateau was used in the subsequent acquisition of perfusion and control weighted images.

Quantification of the inversion efficiency was performed in separate experiments on four animals positioned to image the neck and carotid arteries (Fig. 3). By incorporation of inversion pulses within a two-dimensional gradient-echo sequence (see above) the inversion efficiency of HS and sinc inversion pulses were compared. In all four animals the repetition time at which maximum inversion efficiency occurred was 55 msec (or 55 pulses per three seconds). The mean inversion efficiency over all animals was 0.72 ± 0.04 when sinc inversion pulses were used and 0.79 ± 0.05 when HS pulses were used. From the expanded color overlay of inversion efficiency (Fig. 3) it can be seen that there is a distribution of inversion efficiency across the carotids possibly due to a distribution of flow with a maximum in the center and minimum at the periphery. This distribution is possibly the reason why the relative signal difference plateaus with increasing HS repetition rate (Fig. 2) instead of reaching a clearly defined maximum.

The left column of Fig. 4 shows examples of 16-echo FSE proton density weighted images of a normal rat brain compared breathing the air/isoflurane (a) and carbogen/isoflurane (c) anesthetic mixtures. The corresponding TBF maps are shown on the right (Fig. 4b and d). Similarly, Fig. 5 shows the same sequence of images of a 9L glioma-bearing rat. The hyperintense tumor is clearly evident on the right side of the brain (Fig. 5a and c), which exhibits low flow (Fig. 5b and d). Since these images were acquired with a standard birdcage RF resonator there was no evidence of RF inhomogeneity across the images. Although 16 echoes were used to acquire the images the brain still appears sharp enough

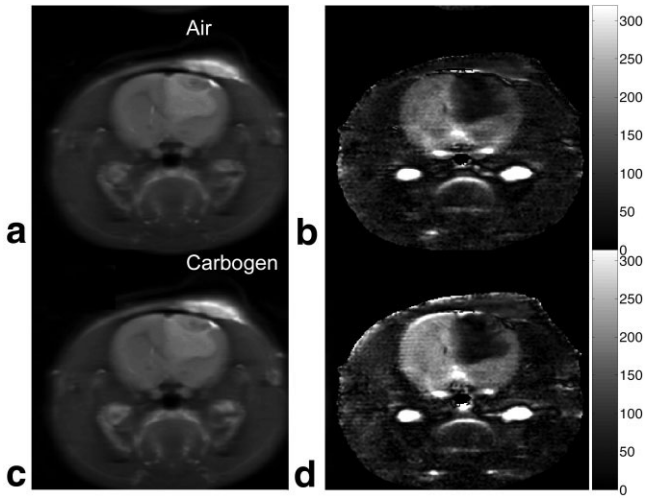

Figure 5. An example of the CASL imaging results for an intracerebral 9L gliosarcoma while the animal was breathing air and isoflurane (**a** and **b**), and while it was breathing carbogen and isoflurane (**c** and **d**). The FSE proton density weighted images with arterial spin tagging by CASL (a and c) are shown on the left, while the corresponding TBF (mL/100 g/minute) images (b and d), are shown on the right.

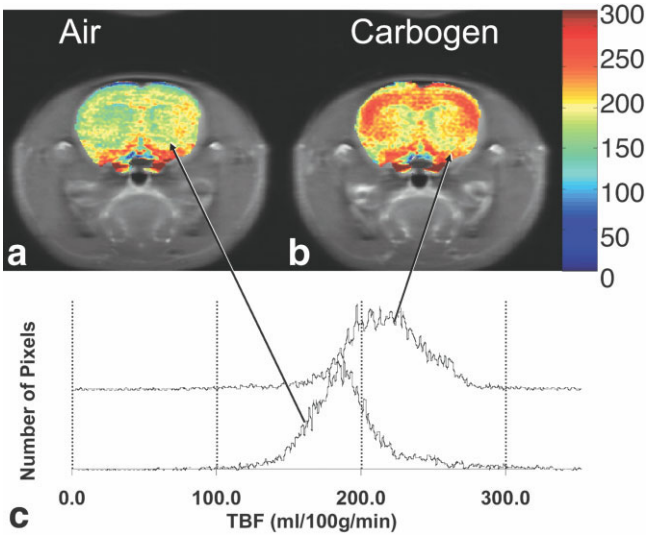

Figure 6. TBF (mL/100 g/minute) color overlays on proton density weighted CASL images of a normal rat brain while the animal was breathing air and isoflurane (**a**), and while it was breathing carbogen and isoflurane mix (**b**). The distribution of blood flow in the brain is shown by a histogram plot of blood flow (**c**). The y axis of the histogram plot represents the relative proportion of the brain with a given blood flow (x axis).

to resolve internal structures. Large blood vessels outside of the brain are heavily blurred due to the FSE sequence, but this does not affect the areas of interest in brain and tumor. Despite some reduction due to MT, the quality of the proton density images remains adequate to depict blood flow features.

The corresponding absolute TBF maps calculated using Eq. [2] are shown in grayscale on the right column of Figs. 4 and 5, and as color overlays in Figs. 6 and 7. In these images the gray/white matter structure within the rat brain can be resolved. Noise in TBF maps was estimated by the SD of 5 × 5 pixel ROIs defined in contralateral to tumor ($N = 5$) and normal brain ($N = 4$) regions. The noise of the TBF maps was determined to be approximately ±10 mL/100 g/minute. Thus SNR of TBF maps was adequate to quantify the heterogeneity of the low blood flow features of this tumor, which ranged from 20 to 100 mL/100 g/minute (Table 1).

As the anesthetic mixture was changed to carbogen/isoflurane (hypercapnic) the change in signal intensity is almost indistinguishable on the proton density images. However, on the TBF maps (Figs. 6 and 7) the effect of the carbogen gas on CBF is clearly evident. From these maps it can qualitatively be seen that the blood flow in the normal rat brain and the rat brain contralateral to the tumor increases significantly when the rat is switched from normocapnic to hypercapnic states. Due to the extremely low flow it is difficult to visualize on TBF maps whether the carbogen has an effect on the blood flow within the tumors (Figs. 5 and 7). Color overlays (Figs. 6 and 7) are helpful in depiction of flow heterogeneity, which is further characterized using histogram analysis.

From the histograms of TBF within brain and tumor (Figs. 6 and 7) the effect of carbogen on brain blood flow is readily apparent. In the normal brain the histogram distribution of flow approximates a Gaussian shape. This distribution shifts and widens to higher flow under the hypercapnic conditions (Fig. 6). However, for the brains with 9L tumors the distribution of blood flow is a bimodal with low and high flow components originating from the tumor and normal brain regions, respectively (Figs. 7 and 8). Note that there is a shift to higher flow in normal brain under hypercapnic conditions; however, the flow in the tumor remains relatively unaffected by the administration of carbogen.

A summary of the experimental results for four normal and five tumor-bearing rats is presented in Table 1. These result indicate that blood flow to both normal rat brain and the contralateral brain increase significantly when the anesthetic mixture contains carbogen instead of air, but the flow to the tumor is largely unaffected. Figure 8 shows using color overlays an example of the ROIs used for calculating the results in Table 1. Definition of subtumor ROIs are somewhat subjective; however, the results are meant for highlighting the heterogeneity of tumor TBF.

DISCUSSION

Tumor viability, oxygenation, and accessibility by blood-delivered anti-cancer agents are dependent on tumor blood flow. Moreover, as anti-angiogenic strategies progress for cancer treatment there is a need to develop imaging protocols adequately sensitive to tumor flow levels. The objective in this work was to develop a sensitive, robust, noninvasive, and quantitative measure of TBF in rodent brain cancer models.

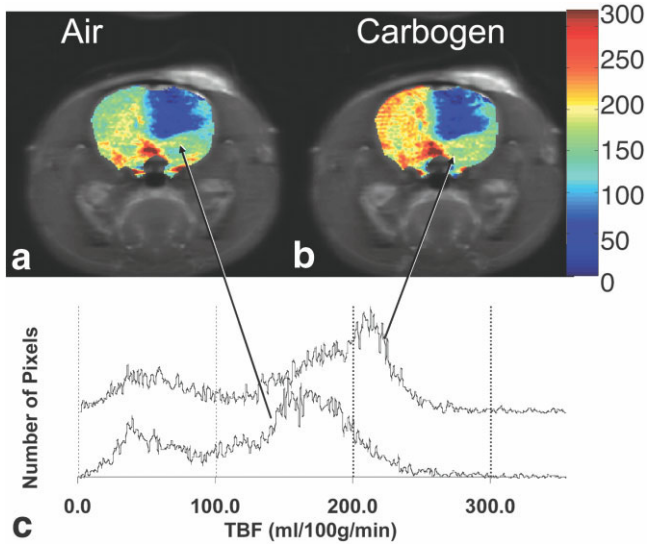

Figure 7. TBF (mL/100 g/minute) color overlays on proton density weighted CASL images of an intracerebral 9L gliosarcoma while the animal was breathing air and isoflurane (**a**), and while it was breathing carbogen and isoflurane (**b**). The bimodal distribution of blood flow in the brain and tumor is shown by a histogram plot of blood flow (**c**). The y axis of the histogram plot represents the relative proportion of the brain with a given blood flow (x axis).

Table 1
Tissue Blood Flow Results

	Air/isoflurane, mean ± SEM (mL/100g/minute)	Carbogen/isoflurane, mean ± SEM	% increase, mean ± SEM
Normal brain ($N = 4$)[a]	166 ± 16	198 ± 17	16 ± 10
Contra-lateral brain ($N = 5$)[b]	138 ± 25	169 ± 31	17 ± 11
Whole tumor ($N = 5$)[b]	43 ± 8	48 ± 13	5 ± 21
Tumor periphery ($N = 5$)[b]	57 ± 11	64 ± 12	8 ± 19
Tumor core ($N = 5$)[b]	29 ± 11	31 ± 9	2 ± 38

[a]Results for a single slice through the brain as exemplified by color overlays in Figure 5.
[b]Results for regions of interest as exemplified by the color overlays in Figure 7.

In the original ASL approach described by Detre et al (4), saturation of blood spins was achieved by a train of spatially selective saturation pulses. However, flow-driven adiabatic inversion of blood spins has since become the preferred method for arterial tagging (5). In this method originally proposed for angiography (11), blood spins flowing along the direction of an applied gradient field continuously change Larmor frequency dependent on position along the gradient axis. As a result, flowing spins undergo adiabatic inversion via a fixed-frequency RF field. The use of CASL for quantification of TBF in rat brain tumors has previously been established and demonstrated to be sensitive enough to measure the low flow distributions present within the tumors (3,7). However, CASL has failed to gain widespread use in monitoring TBF in tumors in pre-clinical or clinical applications, which we expect is partially due to technical complexity.

The CASL sequence developed here maintains the CASL sensitivity to low flow and small flow changes while avoiding some of the technical difficulties of the true CASL methods. Acquisition of good quality flow maps can be achieved using only one volume coil for both excitation and detection of the nuclear magnetic resonance (NMR) signal. MT signal degradation of CASL sequence was moderate (~30%) relative to previous single coil CASL sequences (up to 70%) (12). The source of this MT reduction is likely due to a decrease in the power deposition of the train of HS pulses compared to the "truly" continuous ASL pulse sequences. Given the amplitude of the HS pulses reported here, the duty cycle (3.7%), and the ratio of peak power to mean power (1.56/6.12) of the HS pulses, the total power deposition was estimated to be at least 53% that of the previously reported single coil CASL protocols (9,12). This approach also obviates the need for additional amplifier/coils beyond a basic single RF-channel system. Finally, this approach offers additional practical advantages when other elements of the protocol require a volume coil for multislice imaging, such as in our studies on rodent tumor models. However, a single transmit/receive volume coil may have reduced sensitivity relative to a receive-only surface coil system.

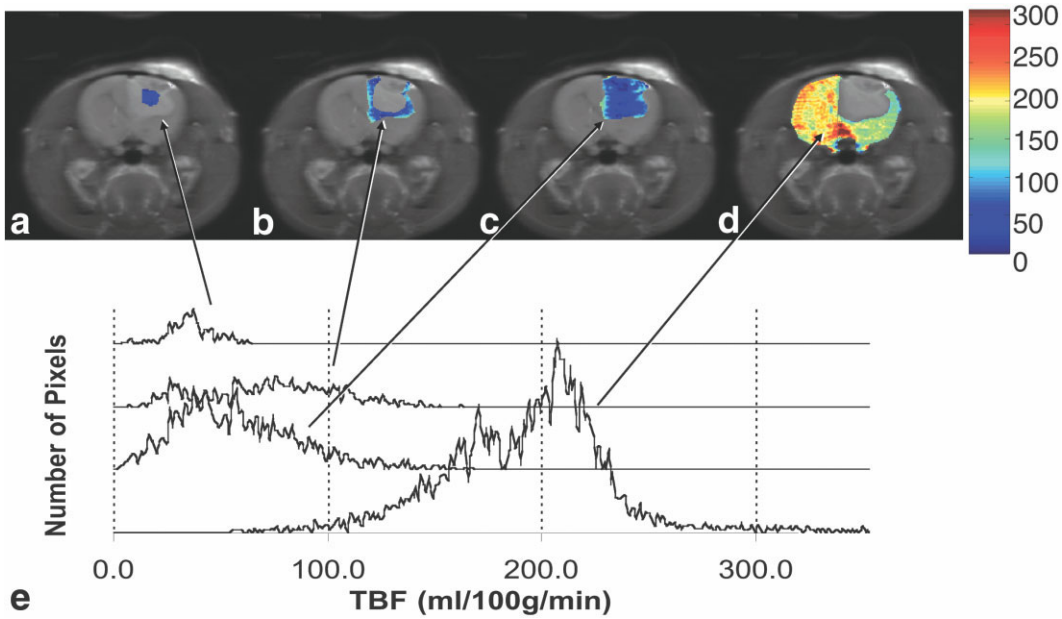

Figure 8. Examples of TBF ROIs for tumor core (**a**), tumor periphery (**b**), whole tumor (**c**), and normal brain tissue (**d**). From the corresponding histogram plots (**e**) it can be seen that the tumor has a significantly slower blood flow than that of the normal brain.

The CASL protocol for measuring TBF was validated here by measuring the blood flow in both normal rat brain and intracerebral 9L gliomas. The mean blood flow in normal rat brain was found to be 166 ± 16 mL/100 g/minute, which is within error of those previously reported in the literature (3,8,9). The measured blood flow within the tumor core (29 ± 11) and periphery (57 ± 11) were also within error of those reported by Silva et al (3).

An important aspect of this sequence is its sensitivity to measure low flows common in brain tumors as demonstrated by CASL protocol applied to the 9L tumor model. Random error in the flow maps was estimated to be approximately 10 mL/100 g/minute, which is less than the mean flow and heterogeneity within the tumor. As summarized in Table 1, the mean flow within the tumor periphery was significantly higher than the tumor core, which is consistent with known physiology of many tumors.

Finally, we demonstrated that this perfusion sequence could quantify dynamic changes in TBF using carbogen (a known vasodilator). The effects of carbogen on TBF distributions within the rat brain were contrasted to TBF data acquired under control conditions. The increase in blood flow to normal brain in response to carbogen is consistent with other studies of the physiologic effects of increased CO_2 levels in normal brain (5,12–14). A quantitative comparison across these studies, including ours, is confounded by reactivity of vasodilators and anesthetics. However, the mean increase in blood flow (16%) reported here is within error of recent studies on rats under similar anesthesia conditions (8). The inability of carbogen to affect a change on blood flow in the 9L tumors is also consistent with previous results (15) indicating that the 9L tumor is relatively vasoinactive.

In conclusion, the described single coil CASL protocol is a simple and robust method to measure blood flow within the rat brain. It has similar inversion efficiency (0.79) to that of other single coil methods (9) without the same degree of MT degradation of image quality. The ability to quantitatively and non-invasively measure blood flow features within a low-flow tumor will facilitate the evaluation experimental tumor therapies in pre-clinical models. This approach offers several practical advantages for integration within other imaging protocols and straightforward implementation on a standard animal MRI system.

REFERENCES

1. Barbier EL, Lamalle L, Decorps M. Methodology of brain perfusion imaging. J Magn Reson Imaging 2001;13:496–520.
2. Wong EC, Buxton RB, Frank LR. A theoretical and experimental comparison of continuous and pulsed arterial spin labeling techniques for quantitative perfusion imaging. Magn Reson Med 1998; 40:348–355.
3. Silva AC, Kim SG, Garwood M. Imaging blood flow in brain tumors using arterial spin labeling. Magn Reson Med 2000;44:169–173.
4. Detre JA, Leigh JS, Williams DS, Koretsky AP. Perfusion imaging. Magn Reson Med 1992;23:37–45.
5. Williams DS, Detre JA, Leigh JS, Koretsky AP. Magnetic resonance imaging of perfusion using spin inversion of arterial water. Proc Natl Acad Sci USA 1992;89:212–216.
6. Kim SG, Tsekos NV. Perfusion imaging by a flow-sensitive alternating inversion recovery (FAIR) technique: application to functional brain imaging. Magn Reson Med 1997;37:425–435.
7. Lei H, Peeling J. A strategy to optimize the signal-to-noise ratio in one-coil arterial spin tagging perfusion imaging. Magn Reson Med 1999;41:563–568.
8. Sicard K, Shen Q, Brevard ME, et al. Regional cerebral blood flow and BOLD responses in conscious and anesthetized rats under basal and hypercapnic conditions: implications for functional MRI studies. J Cereb Blood Flow Metab 2003;23:472–481.
9. Zhang W, Williams DS, Koretsky AP. Measurement of rat brain perfusion by NMR using spin labeling of arterial water: in vivo determination of the degree of spin labeling. Magn Reson Med 1993;29:416–421.
10. Ross BD, Zhao YJ, Neal ER, et al. Contributions of cell kill and posttreatment tumor growth rates to the repopulation of intracerebral 9L tumors after chemotherapy: an MRI study. Proc Natl Acad Sci USA 1998;95:7012–7017.
11. Dixon WT, Du LN, Faul DD, Gado M, Rossnick S. Projection angiograms of blood labeled by adiabatic fast passage. Magn Reson Med 1986;3:454–462.
12. Zhang W, Williams DS, Detre JA, Koretsky AP. Measurement of brain perfusion by volume-localized NMR spectroscopy using inversion of arterial water spins: accounting for transit time and cross-relaxation. Magn Reson Med 1992;25:362–371.
13. Forbes ML, Hendrich KS, Kochanek PM, et al. Assessment of cerebral blood flow and CO2 reactivity after controlled cortical impact by perfusion magnetic resonance imaging using arterial spin-labeling in rats. J Cereb Blood Flow Metab 1997;17:865–874.
14. Barbier EL, Silva AC, Kim SG, Koretsky AP. Perfusion imaging using dynamic arterial spin labeling (DASL). Magn Reson Med 2001;45:1021–1029.
15. Brown SL, Ewing JR, Kolozsvary A, Butt S, Cao Y, Kim JH. Magnetic resonance imaging of perfusion in rat cerebral 9L tumor after nicotinamide administration. Int J Radiat Oncol Biol Phys 1999; 43:627–633.